Drivers of cloud droplet number variability in the summertime Southeast United States

Aikaterini Bougiatioti[1,2], Athanasios Nenes[2,3,4], Jack J. Lin[2,a], Charles A. Brock[5], Joost A. de Gouw[5,6,b], Jin Liao[5,6,c,d], Ann M. Middlebrook[5], André Welti[5,6,e]

[1]Institute for Environmental Research & Sustainable Development, National Observatory of Athens, P. Penteli, GR-15236, Greece
[2]School of Earth & Atmospheric Sciences, Georgia Institute of Technology, Atlanta, GA 30332, USA
[3]Laboratory of Atmospheric Processes and their Impacts, School of Architecture, Civil & Environmental Engineering, École Polytechnique Fédérale de Lausanne, CH-1015, Lausanne, Switzerland
[4]Institute for Chemical Engineering Sciences, Foundation for Research and Technology Hellas, Patras, GR-26504, Greece
[5]Chemical Sciences Division, NOAA Earth System Research Laboratory, Boulder, CO, 80305, USA
[6]Cooperative Institute for Research in Environmental Sciences, Univ. of Colorado, Boulder, CO, 80309, USA
[a] now at: Nano and Molecular Systems Research Unit, Box 3000, FI-90014 University of Oulu, Oulu, Finland
[b] now at: Department of Chemistry and Biochemistry, University of Colorado Boulder, Boulder, CO, USA
[c] now at: Atmospheric Chemistry and Dynamic Laboratory, NASA Goddard Space Flight Center, Greenbelt, MD, USA
[d] now at: Universities Space Research Association, GESTAR, Columbia, MD, USA
[e] now at: Atmospheric Composition Research Unit, Finnish Meteorological Institute, Helsinki, Finland

Correspondence to: Aikaterini Bougiatioti (abougiat@noa.gr), Athanasios Nenes (athanasios.nenes@epfl.ch).

Abstract

Here we analyze regional scale data collected onboard the NOAA WP-3D aircraft during the 2013 Southeast Nexus (SENEX) campaign to study the aerosol-cloud droplet link and quantify the sensitivity of droplet number to aerosol number, chemical composition and vertical velocity. For this, the observed aerosol size distributions, chemical composition and vertical velocity distribution are introduced into a state-of-the-art cloud droplet parameterization to show that cloud maximum supersaturations in the region are low, ranging from 0.02 to 0.52% with an average of 0.14±0.05%. Based on these low values of supersaturation, the majority of activated droplets correspond to particles of dry diameter 90 nm and above. An important finding is that the standard deviation of the vertical velocity (σ_w) exhibits considerable diurnal variability (ranging from 0.16 m s^{-1} during nighttime to over 1.2 m s^{-1} during day) and it tends to covary with total aerosol number (N_a). This σ_w-N_a covariance amplifies the predicted response in cloud droplet number (N_d) to N_a increases by 3 to 5 times - which is important, given that droplet formation is often velocity-limited, and therefore should normally be insensitive to aerosol changes. We also find that N_d cannot exceed a characteristic concentration that depends solely on σ_w. Correct consideration of σ_w and its covariance with time and N_a is important for fully understanding aerosol-cloud interactions and the magnitude of the aerosol indirect effect. Given that model assessments of aerosol–cloud-climate

interactions do not routinely evaluate for overall turbulence or its covariance with other parameters, datasets and analyses such as the one presented here are of the highest priority to address unresolved sources of hydrometeor variability, bias, and the response of droplet number to aerosol perturbations.

1. Introduction

Atmospheric particles (aerosols) interact with incoming solar radiation and tend to cool the Earth, especially over dark surfaces such as oceans and forests (Charlson et al., 1992; Seinfeld and Pandis, 1998). Aerosols also act as cloud condensation nuclei (CCN), form droplets in clouds and indirectly affect climate by modulating precipitation patterns and cloud radiative properties. Aerosol-cloud interactions constitute the most uncertain aspects of anthropogenic climate change (Seinfeld et al., 2016). Studies often highlight the importance of constraining the aerosol size distribution, particle composition and mixing state for predicting CCN concentrations (Cubison et al., 2008; Quinn et al., 2008; Riemer et al., 2019). Model assumptions often cannot consider the full complexity required to comprehensively compute CCN – which together with other emissions and process uncertainties lead to CCN prediction errors that can be significant (e.g., Fanourgakis et al., 2019). Owing to the sublinear response of cloud droplet number concentration (N_d) to aerosol perturbations, prediction errors in CCN generally result in errors in N_d which are less than those for CCN (Fanourgakis et al., 2019). The sublinear response arises because elevated CCN concentration generally increases the competition of the potential droplets for water vapor; this in turn depletes supersaturation and the N_d that can eventually form (Reutter et al., 2009; Bougiatioti et al., 2016; Fanourgakis et al., 2019; Kalkavouras et al., 2019). A critically important parameter is the vertical velocity, as it is responsible for generation of supersaturation that drives droplet formation and growth. Droplet number variability may be driven primarily by vertical velocity variations (Kacarab et al., 2020; Sullivan et al., 2019). Compared to aerosols, vertical velocity is much less observed, constrained and evaluated in aerosol-cloud interaction studies, hence may be a source of persistent biases in models (Sullivan et al., 2019).

The Southeast United States (SEUS) presents a particularly interesting location for studying regional climate change, as it has not considerably warmed over the past 100 years – except during the last decade (Carlton et al., 2018; Yu et al., 2014; Leibensperger et al., 2012a,b). These trends are in contrast with the trends observed in most locations globally (IPCC 2013), and several hypotheses have been proposed to explain this regional phenomenon, including the effect of involving short-lived climate forcers such as secondary aerosols combined with the enhanced humidity in the region and their impact on clouds (Carlton et al., 2018; Yu et al., 2014). Here, we analyze data collected during the Southeast Nexus of Air Quality and Climate (SENEX) campaign in June-July 2013, which was the airborne component led by the National Oceanic and Atmospheric Administration (NOAA), of a greater measurement campaign throughout the

SEUS, the Southeast Atmosphere Study (SAS; Carlton et al., 2018). Here we analyze data collected onboard the NOAA WP-3D and apply a state-of-the-art droplet parameterization to determine the maximum supersaturation and N_d achieved in cloudy updrafts, for all science flights with available number size distribution and chemical composition data. We also determine the sensitivity of droplet formation to vertical velocity and aerosol, with the purpose of understanding the drivers of droplet variability in the boundary layer of the SEUS by obtaining regional-scale, representative values of the relationship between the driving parameters and cloud droplet number.

2. Methods

2.1 Aircraft instrumentation

The analysis utilizes airborne, in situ data collected during the June-July 2013 SENEX mission, aboard the National Oceanic and Atmospheric Administration (NOAA) WP-3D aircraft (typical airspeed ~100 m s^{-1}) based in Smyrna, Tennessee (36º00'32''N, 86º31'12''W). In total, twenty research flights were conducted. Based on the availability of the relevant data described below, thirteen flights are analyzed in this work. Table 1 provides a synopsis of the analyzed research flights where times are local (UTC-5). Detailed information on the instrumentation and measurement strategy during the SENEX campaign is provided by Warneke et al. (2016).

Dry particle number distributions from 4 - 7000 nm were measured using multiple condensation and optical particle counters. 4-700 nm particles were measured by a nucleation mode aerosol size spectrometer (NMASS; Warneke et al., 2016) and an ultra-high sensitivity aerosol spectrometer (UHSAS; Brock et al., 2011), while for larger particles with dry diameters between 0.7 and 7.0 μm, a custom-built white-light optical particle counter (WLOPC) was used (Brock et al., 2011).

Measurements of the composition of submicron (< 0.7 μm vacuum aerodynamic diameter) non-refractory particles were made with a compact time-of-flight aerosol mass spectrometer (C-ToF-AMS; Aerodyne, Billerica, Massachesetts, US) (Canagaratna et al., 2007; Kupc et al., 2018) customized for aircraft use, with a 10 s time resolution (Warneke et al., 2016). Particles entering the instrument are focused and impacted on a 600 ºC inverted-cone vaporizer. The volatilized vapors are analyzed by electron ionization mass spectrometry, providing mass loadings of sulfate, nitrate, organics, ammonium and chloride. For the C-ToF-AMS, the transmission efficiency of particles between 100 and 700 nm is assumed to be 100% through the specific aerodynamic focusing lens used while mass concentrations are calculated using a chemical composition-dependent collection efficiency (Middlebrook et al., 2012; Wagner et al., 2015). The C-ToF-AMS measures only non-refractory aerosol chemical composition, therefore this analysis provides mass

loadings of sulfate, nitrate, ammonium and organic constituents with a 10 s time resolution and neglects the contribution of black carbon (BC). The calculation of the average volume fractions from the mass loading follows that of Moore et al. (2012). An average organic density of 1.4 g cm^{-3} is used, characteristic of aged aerosol (Moore et al., 2011; Lathem et al., 2013) while for the inorganic species the respective densities are used, assuming the aerosol to be internally mixed.

The aircraft was equipped by the NOAA Aircraft Operations Center (AOC) flight facility with a suite of instruments to provide information on exact aircraft position as well as numerous meteorological parameters (Warneke et al., 2016). The analysis in this work makes use of vertical wind velocity, aircraft pressure altitude, and ambient temperature, pressure and relative humidity (RH) provided by NOAA AOC. The location of the instrumentation on the aircraft is described elsewhere (Warneke et al., 2016). For measurements inside the fuselage, a low turbulence inlet (Wilson et al., 2004) and sampling system (Brock et al., 2011; 2016a) was used to decelerate the sample flow to the instruments. The C-ToF-AMS was connected downstream of an impactor with 50% efficiency at a 1.0 μm aerodynamic diameter (PM1) cut-point (Warneke et al., 2016).

2.2 Aerosol hygroscopicity parameter

The aerosol hygroscopicity parameter (Petters and Kreidenweis, 2007), κ, is calculated assuming a mixture of an organic and inorganic component with volume fractions ε_{org}, ε_{inorg} and characteristic hygroscopicities κ_{org}, $\kappa_{inorg,}$ respectively ($\kappa=\varepsilon_{inorg}\kappa_{inorg}+\varepsilon_{org}\kappa_{org}$). The organic and inorganic volume fraction are derived from the C-ToF-AMS data. Since throughout the summertime SEUS, aerosol inorganic nitrate mass and volume fraction are very low (Weber et al., 2016; Fry et al., 2018), κ_{inorg}=0.6, representative for ammonium sulfate, is used. For the organic fraction, a hygroscopicity value of κ_{org}=0.14 is used, based on concurrent measurements conducted at the ground site of the SAS at the rural site of Centreville, Alabama (Cerully et al., 2015). This value is also in accordance with the cumulative result of studies conducted in the Southeast US using measurements of droplet activation diameters in subsaturated regimes, providing κ_{org} of > 0.1 (Brock et al., 2016a).

2.3 Cloud droplet number and maximum supersaturation

Using the observed aerosol number size distribution (1 s time resolution), the hygroscopicity derived from the chemical composition measurements (10 s time resolution) and vertical velocity, we calculate the (potential) cloud droplet number (N_d) and maximum supersaturation (S_{max}) that would form in clouds in the airmasses sampled. Droplet number and maximum supersaturation calculations are carried out using an approach similar to that of Bougiatioti et al. (2016) and Kalkavouras et al. (2019) with the sectional

parameterization of Nenes and Seinfeld (2003), later improved by Barahona et al. (2010) and Morales Betancourt and Nenes (2014a). A sectional representation of the size distribution is used for each 1-s data point (e.g. for Flight 5, n=23213 data points). Given that chemical composition is provided with a 10 s time resolution, the same hygroscopicity values are used for 10 successive size distributions throughout the flight. Temperature and pressure required for droplet number calculations are obtained from the NOAA AOC flight facility dataset.

Given that vertical velocity varies considerably inside the boundary layer, we obtain a droplet number that is representative of the vertical velocity distribution – the average concentration that results from integrating over the distribution (probability density function, PDF) of observed updraft velocities. To accomplish this, each flight is divided into segments where the aircraft flew at a constant height. For each segment, the non-negative vertical velocities are fit to the positive half of a Gaussian distribution with mean of zero and standard deviation σ_w. Only positive vertical velocities ("updrafts") were used in this fit, as they are the part of the vertical velocity spectrum that is responsible for cloud droplet formation. The σ_w values derived from the level leg segments are then averaged into one single σ_w value (and standard deviation) to represent each flight. The PDF-averaged droplet number concentration is then obtained using the "characteristic velocity" approach of Morales and Nenes (2010), where applying the droplet parameterization at a single "characteristic" velocity, $w^*=0.79\sigma_w$ (Morales and Nenes, 2010) gives directly the PDF-averaged value. The flight-averaged σ_w and subsequently the respective w^* is applied to each size distribution measured. Apart from its theoretical basis, this methodology has shown to provide good closure with observed droplet numbers in ambient clouds (e.g. Kacarab et al., 2020).

In determining σ_w, we consider horizontal segments most likely to be in the boundary layer. 91% of the segments are below 1000 m above sea level (mean altitude ~700 m; Table 2 and SP3 for all flights), within the boundary layer in the summertime US (Seidel et al., 2013). The vertical velocity distributions observed gave σ_w =0.97±0.21 m s^{-1} for daytime flights, and σ_w =0.23±0.04 m s^{-1} for nighttime flights (Table 2 and SP3).

Potential droplet formation is evaluated at four characteristic velocities w^* that cover the observed range in σ_w, namely 0.1, 0.3, 0.6, and 1 m s^{-1}. The σ_w = 0.3 m s^{-1} case is most representative of nighttime conditions, while σ_w = 1 m s^{-1} should is most representative of the daytime boundary layer.

We also compute the variance of the derived N_d, estimated from the sensitivity to changes in aerosol number concentration N_a, κ and σ_w, expressed by the partial derivatives $\partial N_d/\partial N_a$, $\partial N_d/\partial \kappa$ and $\partial N_d/\partial \sigma_w$ computed from the parameterization using a finite difference approximation (Bougiatioti et al., 2017; Kalkavouras et al., 2019) using:

$$\sigma^2 N_d = \left(\overline{\frac{\partial N_d}{\partial N_a}}\ \sigma N_a\right)^2 + \left(\overline{\frac{\partial N_d}{\partial \kappa}}\ \sigma\kappa\right)^2 + \left(\overline{\frac{\partial N_d}{\partial \sigma_w}}\ \sigma\sigma_w\right)^2$$

These sensitivities, together with the observed variance in N_a, κ, and σ_w are also used to attribute droplet number variability to variations in the respective aerosol and vertical velocity parameters following the approach of Bougiatioti et al. (2017) and Kalkavouras et al. (2019):

$$\varepsilon_{N\alpha} = \frac{\left(\overline{\frac{\partial N_d}{\partial N_a}}\ \sigma N_a\right)^2}{\sigma^2 N_d}, \varepsilon_{\kappa} = \frac{\left(\overline{\frac{\partial N_d}{\partial \kappa}}\ \sigma\kappa\right)^2}{\sigma^2 N_d}, \varepsilon_{\sigma w} = \frac{\left(\overline{\frac{\partial N_d}{\partial \sigma_w}}\ \sigma\sigma_w\right)^2}{\sigma^2 N_d}$$

3. Results and Discussion

3.1. Particle composition and size distribution

For the determination of the different aerosol species present, neutral and acidic sulfate salts are distinguished by the molar ratio of ammonium to sulfate ions in the aerosol. A molar ratio higher than 2 indicates the presence of only ammonium sulfate, while values between 1 and 2 indicate a mixture of ammonium sulfate and bisulfate (Seinfeld and Pandis, 1998). For most flights, the molar ratio of ammonium versus sulfate was above 2 (mean value 2.41±0.72 and median of 2.06). For the nighttime flights, the values were somewhat lower (mean value 1.91±0.42 and median of 1.85). Nevertheless, ammonium sulfate is always the predominant sulfate salt. Organic mass fractions for the SENEX research flights are provided in Table 1. Overall, organic aerosol dominated the composition during all flights, contributing 66%-75% of the total aerosol volume. Most of the remaining aerosol volume consisted of ammonium sulfate, ranging from 12%-39% (with a mean of 23%±6%). The organic mass fraction during the flights varied with height (see Figure 1). This vertical variability of the chemical composition can have a strong impact on droplet number within the boundary layer, as air masses from aloft may descend and interact with that underneath. Figure 1 represents the organic mass fractions during Flights 6, 12 and 16, with all flights provided in the supplementary material (Figure S1). The lowest organic mass fractions overall were observed during Flight 12 (36%±10% with values almost two-fold higher for altitudes >3000 m, Fig. 1b) while the highest organic mass fractions were observed during flights over predominantly rural areas (Flights 5, 10, and 16 (Fig. 1c)). During Flight 5 the organic mass fraction was high (68%±5%), with the highest values found in the free troposphere at altitudes >3000 m, as was the case for 4 other flights (5/13 in total, Fig. S1). High organic mass fractions were also found during nighttime Flight 9 that included portions of the Atlanta metropolitan area, with values up to 78%. The impact of the aerosol composition variability on droplet number is discussed in section 3.2.

The predominance of the organic fraction is also reflected in the hygroscopicity parameter values, with an overall $\kappa = 0.25 \pm 0.05$, close to the proposed global average of 0.3 (Pringle et al., 2010). The highest values of κ, as expected are observed during flights exhibiting the lowest organic mass fraction, namely Flight 12 with a $\kappa = 0.39$ (Table 1). The rest of the κ-values are close to the overall value of 0.25, corresponding to an organic mass fraction of around 0.60.

Median aerosol size distributions and the respective total aerosol number are obtained from the median and interquartile range in each size bin from the aerosol size distribution measurements during segments where the aircraft flew at a constant height. Aerosol size distributions and changes in them during each flight are crucial as they are used as input for the droplet number parameterization. Overall, N_a ranged from around 500 to over 100000 cm^{-3} with number size distributions varying markedly over the course of a flight (Figure 2). Free tropospheric distributions exhibited characteristics of a bimodal distribution with a prominent broad accumulation mode peak (80-200 nm) and an Aitken mode peak (30-60 nm) (Fig. 2a) while boundary layer size distributions exhibited a more prominent accumulation mode (Fig. 2b). There was considerable variability in the contributions of the nucleation, Aitken, and accumulation modes to total N_a, depending on altitude and proximity to aerosol sources (Fig. 2c). Nevertheless, the modal diameters did not vary considerably, dictating that mostly particles in the same mode will activate, depending on the developed supersaturation. Distributions during nighttime flights exhibited similar N_a and variability between them; nevertheless, size distributions were more complex - exhibiting up to three distinct modes (20-40, 70-100 and 130-200 nm; Fig. 2d).

3.2 Potential cloud droplet number and maximum supersaturation

We first focus on calculation of the potential N_d and S_{max} for data from all thirteen research flights and for the four prescribed values σ_w that represent the observed range. These calculations help understand the sensitivity of droplet formation to N_a and κ for all the airmasses sampled – without considering the added variability induced by changes in turbulence expressed by σ_w (considered later). Results from this analysis are provided in Table 3. The highest N_d were found for Flights 6 and 10, which correspond to ambient conditions with the highest N_a, consistent with the sampling of the Atlanta urban environment. For a given σ_w, the variance of N_d is predominantly caused by changes in N_a rather than changes in hygroscopicity (i.e., chemical composition). The highest influence of κ to N_d variability is found for Flight 18 (12% and 35% for 0.1 and 0.3 m s^{-1}, respectively), during which N_a was the low, and the organic mass fraction was ~50%. The contribution of κ to the N_d variability is as high as 37% (for 0.6 m s^{-1}); despite this large contribution, droplet formation is usually considerably more sensitive to changes in aerosol concentration than to variations in composition. Overall, the relative contribution of the hygroscopicity to the variation of N_d increases from 5±3% for σ_w =0.1 m s^{-1}, to 12.3±8% for σ_w =0.3 m s^{-1}, to 14.5±10% for σ_w =0.3 m s^{-1} and

16.5±9% for σ_w =1 m s^{-1}. As σ_w increases, so does supersaturation and consequently N_d. On average, N_d increases by 62% as σ_w increased from 0.1 to 0.3 m s^{-1}, 70% as σ_w increased from 0.3 to 0.6 m s^{-1} and another 39% as σ_w increased from 0.6 to 1 m s^{-1}. Tripling σ_w from 0.1 to 0.3 m s^{-1} results in 31% increase in S_{max}, while doubling σ_w from 0.3 to 0.6 m s^{-1} results in 26.2% increase in S_{max} and a further σ_w increase to 1 m s^{-1} leads to an additional 20.7% increase in S_{max}.

Considering the changes in vertical velocity between flights (Table 4), we observe that average σ_w during daytime varied little between flights and was large, ranging between 0.85 and 1.2 m s^{-1} with a mean of 0.97±0.21 m s^{-1}. Under such conditions, water availability during droplet formation is aerosol-limited, so that N_d is sensitive to N_a. The degree of water availability is expressed by the S_{max}, which for all the evaluated SENEX data, is 0.14±0.05%. This level of maximum supersaturation activates particles of roughly >90 nm diameter (e.g., accumulation mode particles) into cloud droplets. The highest S_{max} ranged from 0.2 to 0.3% and was found during flights which exhibited large and highly variable σ_w (Flights 4, 5, 12 and 19) while the lowest S_{max} was below 0.10% and was found during nighttime flights (Flights 9, 15 and 16). Contrasts in droplet formation between day and nighttime conditions may be driven primarily by the total aerosol number in the accumulation mode, and not be affected by ultrafine particles.

The large diurnal variability in σ_w (from 0.3 m s^{-1} at night to 1.0 m s^{-1} at day) contributes considerably to the diurnal variability in N_d. To understand the relative importance of all parameters affecting droplet formation (σ_w, N_a, κ) we estimate their contribution to the total variability in N_d based on the variances of κ, N_a and σ_w and the sensitivity of droplet formation to those parameters. The results of the analysis is summarized in Table 4. The σ_w variation during nighttime, although small (always less than 10%), consistently remains an important contributor to N_d variability, because droplet formation tends to be in the updraft velocity-limited regime. At higher values of σ_w (Table 4), the contribution of N_a variability becomes a relatively dominant contributor to N_d variability.

Another way to express the importance of vertical velocity and aerosol number for the levels of droplet number is to compare flights where aerosol number or σ_w vary in a similar way. For this, we focus on two day/night flight pairs (Flights 5 and 15, and Flights 6 and 9), shown in Fig. 3. The first pair of flights were conducted over a rural area under moderate aerosol number conditions, while the second pair exhibited somewhat higher aerosol numbers owing to its proximity to the Atlanta metropolitan area. The size of the markers in Fig.3 represents the potential number of droplets in clouds forming in each airmass sampled, while their color reflects the respective total aerosol number. In both pairs of flights, σ_w varies about the same between night and day (Table 4). For the Flights 5, 15 pair, the difference in N_d between day and night (which is 69% higher during daytime) is driven primarily by aerosol characteristics (69% by N_a and 7% from κ) and only 24% by σ_w. For nighttime (Flight 15), the variability in N_d is driven 58% by aerosol (51%

by N_a and 7% from κ) and 42% by σ_w. For the second pair of night/day flights (Flights 6, 9), N_a is on average similar, σ_w varies by a factor of 4.0 between day and night and κ varies by 13%.

The difference in N_d between day and night (where daytime values are 72.1% higher than nighttime) is almost equally driven by N_a and σ_w changes during the day (54% and 43% respectively), while predominantly driven by N_a during the night (76%; Table 4). Overall, in the proximity of an urban environment with higher aerosol concentrations, 57% of the N_d variability is driven by aerosol (N_a and κ) during the day and 83% during the night. Figure 3 presents the calculated N_d for the four aforementioned flights, namely Flights 5 (Fig. 3a), 15 (Fig. 3b), 6 (Fig. 3c) and 9 (Fig. 3d) using the observed σ_w. The size of the markers represents the estimated number of droplets, while the color scale the respective total aerosol number. Droplet number is lower during nighttime owing to the limited turbulence, i.e., lower σ_w.

Figure 4 shows N_d relative to N_a for flights conducted in the two aforementioned areas, during day (Flights 5 and 15) and night (Flights 6 and 9). For high enough N_a, N_d becomes insensitive to additional amounts of aerosol and reaches a "limiting" N_d, which Kacarab et al. (2020) denotes as N_d^{lim}. This limit in N_d is reached when the competition for water vapor to form droplets is strong enough to inhibit the formation of droplets with further increase in N_a. The intense competition for water vapor is reflected in the low value of S_{max}, which drops below 0.1% when N_d is in the vicinity of N_d^{lim} (Figure 4). The availability of water vapor during droplet formation is driven by σ_w, hence droplet formation is limited by σ_w and thus by velocity, when N_d approaches N_d^{lim}. Figure 5 illustrates these effects, by presenting the relationship between N_a and N_d for "low" w^* (<0.25 ms^{-1}; upper panel), "medium" w^* (0.5-0.7 ms^{-1}; middle panel), and "high" w^* (0.75-1 ms^{-1}; lower panel) for all flights. Under low w^* conditions, changes in N_a does not result in an important change in N_d, so its value corresponds to N_{lim}. When w^* increases to "medium" values (Figure 5b), then N_d becomes sensitive to N_a, which is further amplified at "high" values of w^* (Figure 5c). The covariance of aerosol number and vertical velocity (Figure S3) means that the latter significantly enhances the inherent response of N_d to N_a, which points to the importance of constraining vertical velocity and its variance to correctly capture the aerosol-cloud droplet relationship in any model. The covariance, also observed in other environments (e.g., Kacarab et al., 2020), may result from a more effective convective transfer of aerosol-rich air to cloud forming regions, but requires further investigation.

Analysis of Figure 4 also shows that N_d^{lim} varies between 1200 cm^{-3} during day and around 350 cm^{-3} during night, which points to its strong dependence on σ_w. Indeed, when the N_d^{lim} for all flights (except Flights 4, 12, for which insufficient aerosol is present to reach N_d^{lim}) is expressed as a function of σ_w, a remarkable correlation emerges between the two parameters (Figure 6). Even more interesting is that this relationship is quantitatively similar to the corresponding N_d^{lim} - σ_w relationship Kacarab et al. (2020) found for biomass burning - influenced boundary layer clouds in the Southeast Atlantic. The implication of the N_d^{lim} - σ_w

relationship, and its potential universality, is that when N_d approaches N_d^{lim}, its variability is a reflection of vertical velocity variability alone, not variability in N_a. This opens up the possibility to infer the vertical velocity distribution from the droplet number concentration retrievals in regions where considerable amounts of aerosol are present.

4. Summary and Conclusions

Measurements of vertical wind velocity, ambient temperature, humidity, aerosol number size distribution and composition in the SEUS obtained during the SENEX 2013 project are used to analyze the drivers of droplet formation. Overall, 13 research flights are studied, covering environments over sectors with different aerosol sources, aerosol number, size distribution, chemical composition and updraft velocity. Aerosol volume is largely dominated by an organic fraction resulting in an estimated hygroscopicity of 0.25±0.05.

Based on the calculation of cloud droplet number concentration (N_d) and maximum supersaturation (S_{max}), we find that at the regional scale, N_d variability is largely driven by fluctuations in N_a (Table 4), in accordance with other recent studies (e.g., Fanourgakis et al., 2019; Kalkavouras et al., 2019; Kacarab et al., 2020). Nonetheless, N_d levels are also sensitive to vertical velocity variations, σ_w; a factor of 4.0 change in σ_w on its own may lead to an almost proportional change in N_d (factor of 3.6). These responses however occur over the diurnal timescale, during which N_a also changes; the covariance between σ_w with N_a enhances the apparent response of N_d to changes in N_a levels by a factor of 5 (Figure 4). In "cleaner" environments where total aerosol number is not impacted by local sources, the relative response of N_d to σ_w is almost twice as great at night than during the day (24% for daytime Flight 5 vs. 42% for nighttime Flight 15). On the other hand, the relative response of N_d to N_a is slightly lower during the night than during the day (51% at night vs. 69% during the day). In environments with elevated concentrations of accumulation-mode particles, the majority of N_d variations can be attributed to changes in N_a and to a lesser extent to changes in σ_w. Variations in chemical composition (expressed by κ) do not contribute substantially to droplet number variability in most cases. As expected, S_{max} partially mitigates the response of N_d to N_a. Overall, maximum supersaturation levels remain quite low (0.14±0.05%) with the lowest levels (0.05±0.1%) estimated closest to surface. As a result, particles with diameters >90 nm were the most substantial contributors to CCN.

Our analysis also reveals the importance of the variance in vertical velocity as a key driver of cloud droplet formation and its variability in the region. When the boundary layer turbulence is low (e.g. during nighttime) and water vapor supersaturations are low, σ_w and its variability, can be as important a contributor to N_d as is N_a. On average, the two variables (N_a and σ_w) contribute almost equally to the variability in N_d, accounting for more than 90% of the variability. This finding is consistent with recent modeling studies

noting the importance of vertical velocity variability as a driver of the temporal variability of global hydrometeor concentration (Morales Betancourt and Nenes, 2014b; Sullivan et al., 2016). Furthermore, the N_d response from changes in N_a is magnified up to 5 times by correlated changes in σ_w. A similar situation was seen in marine boundary layers influenced by biomass burning in the Southeast Atlantic (Kacarab et al., 2020). Finally, we identify an upper limit to the number of droplets that can form in clouds which depends only on σ_w. This upper limit value tends to be achieved near the surface, where N_a tends to be higher. Whenever N_d approaches this upper limit, observed droplet variability is driven by σ_w and as a consequence by vertical velocity changes only.

Many aspects of warm cloud physics and especially droplet formation are known for decades. Ensuring that global models simulate N_d for the "right reasons" (i.e., aerosol variability and/or vertical velocity variability) is critical for constraining aerosol-cloud-climate interactions. Our study provides important constraints on the relationships between σ_w, N_a, potential N_d, and S_{max}, and shows the importance of covariance between σ_w and N_a in controlling the N_d that can result from a given value of σ_w. Given that global model assessments of aerosol–cloud-climate interactions do not evaluate for vertical velocity or its covariance with other parameters, our work shows that this omission can lead to an underappreciated source of hydrometeor variability and bias, and to a biased response and attribution of droplet number to aerosol levels.

Data Availability: The data used in this study can be downloaded from the NOAA public data repository at https://www.esrl.noaa.gov/csd/projects/senex/. The Gaussian fits used for determining σ_w and the droplet parameterization used for the calculations in the study are available from athanasios.nenes@epfl.ch upon request.

Author Contributions: AB and AN designed and initiated the study. Analysis methodology and software were developed and provided by AN. The analysis was carried out by AB and AN, with comments from JJL, CB, AMM. Data curation was provided by AB, JJL, CB, JAG, JL, AMM, AW. The manuscript was written by AB and AN with additional comments provided by JJL, CB, AW, AMM. All authors reviewed the manuscript.

Funding: This study was supported by the Environmental Protection Agency STAR Grant R835410, and the European Research Council, CoG-2016 project PyroTRACH (726165) funded by H2020-EU.1.1. –

Excellent Science. AB also acknowledges support from the Action "Supporting of Postdoctoral Researchers" of the Operational Program "Education and Lifelong Learning" (action's beneficiary: General Secretariat for Research and Technology) and is co-financed by the European Social Fund (ESF) and the Greek State. CAB, JAdG, JL, AMM, and AW were supported in part by NOAA's Health of the Atmosphere and Atmospheric Chemistry, Carbon Cycle, and Climate Programs.

Conflicts of Interest: The authors declare no conflict of interest.

References

Barahona, D., West, R.E.L., Stier, P., Romakkaniemi, S., Kokkola, H., and Nenes, A.: Comprehensively accounting for the effect of giant CCN in cloud activation parameterizations, Atmos. Chem. Phys., 10, 2467–2473, https://doi.org/10.5194/acp-10-2467-2010, 2010.

Bougiatioti, A., Bezantakos, S., Stavroulas, I., Kalivitis, N., Kokkalis, P., Biskos, G., Mihalopoulos, N., Papayannis, A., and Nenes, A.: Biomass-burning impact on CCN number, hygroscopicity and cloud formation during summertime in the eastern Mediterranean, Atmos. Chem. Phys., 16, 7389–7409, https://doi.org/10.5194/acp-16-7389-2016, 2016.

Bougiatioti, A., Argyrouli, A., Solomos, S., Vratolis, S., Eleftheriadis, K., Papayannis, A., and Nenes, A.: CCN activity, variability and influence on droplet formation during the HygrA-Cd campaign in Athens, Atmosphere, 8, 108, https://doi.org/10.3390/atmos8060108, 2017.

Brock, C. A., Cozic, J., Bahreini, R., Froyd, K. D., Middlebrook, A. M., McComiskey, A., Brioude, J., Cooper, O. R., Stohl, A., Aikin, K. C., de Gouw, J. A., Fahey, D. W., Ferrare, R. A., Gao, R. S., Gore, W., Holloway, J. S., Hübler, G., Jefferson, A., Lack, D. A., Lance, S., Moore, R. H., Murphy, D. M., Nenes, A., Novelli, P. C., Nowak, J. B., Ogren, J. A., Peischl, J., Pierce, R. B., Pilewskie, P., Quinn, P. K., Ryerson, T. B., Schmidt, K. S., Schwarz, J. P., Sodemann, H., Spackman, J. R., Stark, H., Thomson, D. S., Thornberry, T., Veres, P., Watts, L. A., Warneke, C., and Wollny, A. G.: Characteristics, sources, and transport of aerosols measured in spring 2008 during the aerosol, radiation, and cloud processes affecting Arctic Climate (ARCPAC) Project, Atmos. Chem. Phys., 11, 2423–2453, 2011.

Brock, C. A., Wagner, N. L., Anderson, B. E., Attwood, A. R., Beyersdorf, A., Campuzano-Jost, P., Carlton, A. G., Day, D. A., Diskin, G. S., Gordon, T. D., Jimenez, J. L., Lack, D. A., Liao, J., Markovic, M. Z., Middlebrook, A. M., Ng, N. L., Perring, A. E., Richardson, M. S., Schwarz, J. P., Washenfelder, R. A., Welti, A., Xu, L., Ziemba, L. D., and Murphy, D. M.: Aerosol optical properties in the

394 southeastern United States in summer – Part 1: Hygroscopic growth, Atmos. Chem. Phys., 16, 4987-
395 5007, https://doi.org/10.5194/acp-16-4987-2016, 2016.
396 Canagaratna, M. R., Jayne, J. T., Jimenez, J. L., Allan, J. D., Alfarra,M. R., Zhang, Q., Onasch, T. B.,
397 Drewnick, F., Coe, H., Middlebrook, A., Delia, A., Williams, L. R., Trimborn, A. M., Northway, M.
398 J., DeCarlo, P. F., Kolb, C. E., Davidovits, P., and Worsnop, D. R.: Chemical and microphysical
399 characterization of ambient aerosols with the aerodyne aerosol mass spectrometer, Mass Spectrom.
400 Rev., 26, 185–222, 2007.
401 Carlton, A.G., J.A. de Gouw, J.L. Jimenez, J.L. Ambrose, A.R. Attwood, S. Brown, K.R. Baker, C. Brock,
402 R.C. Cohen, S. Edgerton, C. Farkas, D. Farmer, A.H. Goldstein, L. Gratz, A. Guenther, S. Hunt, L.
403 Jaeglé, D.A. Jaffe, J. Mak, C. McClure, A. Nenes, T.K.V. Nguyen, J.R. Pierce, S. de Sa, N.E. Selin,
404 V. Shah, S. Shaw, P.B. Shepson, S. Song, J. Stutz, J. Surratt, B.J. Turpin, C. Warneke, R.A.
405 Washenfelder, P.O. Wennberg, and Xianling Zhou: A synthesis of the southeast atmosphere studies:
406 coordinated investigation of fundamental atmospheric chemistry questions, Bull. Am. Meteor. Soc.,
407 https://doi.org/10.1175-BAMS-D-16-0048.1, 2018.
408 Charlson, R.J., Schwartz, S.E., Hales, J.M., Cess, R.D., Coakley Jr., J.A., Hansen, J.E., and Hofmann, D.J.:
409 Climate forcing by anthropogenic aerosols, Science, Vol. 255, Issue 5043, 423-430,
410 https://doi.org/10.1126/science.255.5043.423, 1992.
411 Cubison, M. J., Ervens, B., Feingold, G., Docherty, K. S., Ulbrich, I. M., Shields, L., Prather, K., Hering,
412 S., and Jimenez, J. L.: The influence of chemical composition and mixing state of Los Angeles urban
413 aerosol on CCN number and cloud properties, Atmos. Chem. Phys., 8, 5649-5667,
414 https://doi.org/10.5194/acp-8-5649-2008, 2008.
415 DeCarlo, P. F., Kimmel, J. R., Trimborn, A., Northway, M. J., Jayne, J. T., Aiken, A. C., Gonin, M., Fuhrer,
416 K., Horvath, T., Docherty, K. S., Bates, D. R., and Jimenez, J. L.: Field-deployable, high-resolution,
417 time-of-flight aerosol mass spectrometer, Anal. Chem., 78, 8281–8289,
418 https://doi.org/doi:8210.1021/ac061249n, 2006.
419 Fanourgakis, G. S., Kanakidou, M., Nenes, A., Bauer, S. E., Bergman, T., Carslaw, K. S., Grini, A.,
420 Hamilton, D. S., Johnson, J. S., Karydis, V. A., Kirkevåg, A., Kodros, J. K., Lohmann, U., Luo, G.,
421 Makkonen, R., Matsui, H., Neubauer, D., Pierce, J. R., Schmale, J., Stier, P., Tsigaridis, K., van Noije,
422 T., Wang, H., Watson-Parris, D., Westervelt, D. M., Yang, Y., Yoshioka, M., Daskalakis, N., Decesari,
423 S., Gysel-Beer, M., Kalivitis, N., Liu, X., Mahowald, N. M., Myriokefalitakis, S., Schrödner, R.,
424 Sfakianaki, M., Tsimpidi, A. P., Wu, M., and Yu, F.: Evaluation of global simulations of aerosol
425 particle and cloud condensation nuclei number, with implications for cloud droplet formation, Atmos.
426 Chem. Phys., 19, 8591–8617, https://doi.org/10.5194/acp-19-8591-2019, 2019.

Fry, J. L., Brown, S. S., Middlebrook, A. M., Edwards, P. M., Campuzano-Jost, P., Day, D. A., Jimenez, J. L., Allen, H. M., Ryerson, T. B., Pollack, I., Graus, M., Warneke, C., de Gouw, J. A., Brock, C. A., Gilman, J., Lerner, B. M., Dubé, W. P., Liao, J., and Welti, A.: Secondary organic aerosol (SOA) yields from NO3 radical + isoprene based on nighttime aircraft power plant plume transects, Atmos. Chem. Phys., 18, 11663-11682, https://doi.org/10.5194/acp-18-11663-2018, 2018.

Cerully, K. M., Bougiatioti, A., Hite, Jr., J. R., Guo, H., Xu, L., Ng, N. L., Weber, R., and Nenes, A.: On the link between hygroscopicity, volatility, and oxidation state of ambient and water-soluble aerosols in the southeastern United States, Atmos. Chem. Phys., 15, 8679–8694, 2015, https://doi.org/10.5194/acp-15-8679-2015.

IPCC (Intergovernmental Panel on Climate Change): Climate Change 2013: The Physical Science Basis, Summary for Policymakers, Cambridge University Press, Cambridge, UK and New York, 2013.

Kacarab, M., Thornhill, K. L., Dobracki, A., Howell, S. G., O'Brien, J. R., Freitag, S., Poellot, M. R., Wood, R., Zuidema, P., Redemann, J., and Nenes, A.: Biomass burning aerosol as a modulator of the droplet number in the southeast Atlantic region, Atmos. Chem. Phys., 20, 3029–3040, https://doi.org/10.5194/acp-20-3029-2020, 2020.

Kalkavouras, P., Bossioli, E., Bezantakos, S., Bougiatioti, A., Kalivitis, N., Stavroulas, I., Kouvarakis, G., Protonotariou, A. P., Dandou, A., Biskos, G., Mihalopoulos, N., Nenes, A., and Tombrou, M.: New particle formation in the southern Aegean Sea during the Etesians: importance for CCN production and cloud droplet number, Atmos. Chem. Phys., 17, 175-192, https://doi.org/10.5194/acp-17-175-2017, 2017.

Kalkavouras, P., Bougiatioti, A., Kalivitis, N., Stavroulas, I., Tombrou, M., Nenes, A., and Mihalopoulos, N.: Regional new particle formation as modulators of cloud condensation nuclei and cloud droplet number in the eastern Mediterranean, Atmos. Chem. Phys., 19, 6185–6203, https://doi.org/10.5194/acp-19-6185-2019, 2019.

Kupc, A., Williamson, C., Wagner, N. L., Richardson, M., and Brock, C. A.: Modification, calibration, and performance of the Ultra-High Sensitivity Aerosol Spectrometer for particle size distribution and volatility measurements during the Atmospheric Tomography Mission (ATom) airborne campaign, Atmos. Meas. Tech., 11, 369–383, https://doi.org/10.5194/amt-11-369-2018, 2018.

Lathem, T. L., Beyersdorf, A. J., Thornhill, K. L., Winstead, E. L., Cubison, M. J., Hecobian, A., Jimenez, J. L., Weber, R. J., Anderson, B. E., and Nenes, A.: Analysis of CCN activity of Arctic aerosol and Canadian biomass burning during summer 2008, Atmos. Chem. Phys., 13, 2735-2756, https://doi.org/10.5194/acp-13-2735-2013, 2013.

Leibensperger, E. M., Mickley, L. J., Jacob, D. J., Chen, W.-T., Seinfeld, J. H., Nenes, A., Adams, P. J., Streets, D. G., Kumar, N., and Rind, D.: Climatic effects of 1950–2050 changes in US anthropogenic

aerosols – Part 1: Aerosol trends and radiative forcing, Atmos. Chem. Phys., 12, 3333-3348, https://doi.org/10.5194/acp-12-3333-2012, 2012a.

Leibensperger, E. M., Mickley, L. J., Jacob, D. J., Chen, W.-T., Seinfeld, J. H., Nenes, A., Adams, P. J., Streets, D. G., Kumar, N., and Rind, D.: Climatic effects of 1950–2050 changes in US anthropogenic aerosols – Part 2: Climate response, Atmos. Chem. Phys., 12, 3349-3362, https://doi.org/10.5194/acp-12-3349-2012, 2012b.

Middlebrook, A. M., Bahreini, R., Jimenez, J. L., and Canagaratna, M. R.: Evaluation of composition-dependent collection efficiencies for the Aerodyne aerosol mass spectrometer using field data, Aerosol Sci. Tech., 46, 258–271, doi.org/10.1080/02786826.2011.620041, 2012.

Moore, R. H., Bahreini, R., Brock, C. A., Froyd, K. D., Cozic, J., Holloway, J. S., Middlebrook, A. M., Murphy, D. M., and Nenes, A.: Hygroscopicity and composition of Alaskan Arctic CCN during April 2008, Atmos. Chem. Phys., 11, 11 807–11 825, https://doi.org/10.5194/acp-11-11807-2011, 2011.

Moore, R. H., Cerully, K., Bahreini, R., Brock, C. A., Middlebrook, A. M., and Nenes, A.: Hygroscopicity and composition of California CCN during summer 2010, J. Geophys. Res., 117, https://doi.org/10.1029/2011JD017352, 2012.

Morales, R. and Nenes, A.: Characteristic updrafts for computing distribution-averaged cloud droplet number, autoconversion rate effective radius, J. Geophys. Res., 115, D18220, doi:10.1029/2009JD013233, 2010.

Morales Betancourt, R. and Nenes, A.: Droplet activation parameterization: the population-splitting concept revisited, Geosci. Model Dev., 7, 2345–2357, https://doi.org/10.5194/gmd-7-2345-2014, 2014a.

Morales Betancourt, R. and Nenes, A.: Understanding the contributions of aerosol properties and parameterization discrepancies to droplet number variability in a global climate model, Atmos. Chem. Phys., 14, 4809-4826, https://doi.org/10.5194/acp-14-4809-2014, 2014b.

Nenes, A. and Seinfeld, J.H.: Parameterization of cloud droplet formation in global climate models, J. Geophys. Res, 108, 4415, doi:10.1029/2002JD002911, 2003.

Petters, M. D. and Kreidenweis, S. M.: A single parameter representation of hygroscopic growth and cloud condensation nucleus activity, Atmos. Chem. Phys., 7, 1961–1971, doi:10.5194/acp-7-1961-2007, 2007.

Pringle, K. J., Tost, H., Pozzer, A., Pöschl, U., and Lelieveld, J.: Global distribution of the effective aerosol hygroscopicity parameter for CCN activation, Atmos. Chem. Phys., 10, 5241–5255, https://doi.org/10.5194/acp-10-5241-2010, 2010.

493 Quinn, P. K., Bates, T. S., Coffman, D. J., and Covert, D. S.: Influence of particle size and chemistry on
494 the cloud nucleating properties of aerosols, Atmos. Chem. Phys., 8, 1029-1042,
495 https://doi.org/10.5194/acp-8-1029-2008, 2008.
496 Reutter, P., Su, H., Trentmann, J., Simmel, M., Rose, D., Gunthe, S. S., Wernli, H., Andreae, M. O., and
497 Pöschl, U.: Aerosol- and updraft-limited regimes of cloud droplet formation: influence of particle
498 number, size and hygroscopicity on the activation of cloud condensation nuclei (CCN), Atmos. Chem.
499 Phys., 9, 7067-7080, https://doi.org/10.5194/acp-9-7067-2009, 2009.
500 Riemer, N., Ault, A. P., West, M., Craig, R. L., & Curtis, J. H.: Aerosol mixing state: Measurements,
501 modeling, and impacts. Reviews of Geophysics, 57, 187–249. https://doi.org/10.1029/2018RG000615,
502 2019
503 Seidel, D. J., Zhang, Y., Beljaars, A., Golaz, J.-C., Jacobson, A. R., and Medeiros, B.: Climatology of the
504 planetary boundary layer over the continental United States and Europe, J. Geophys. Res., 117,
505 D17106, doi:10.1029/2012JD018143, 2013.
506 Seinfeld, J., and Pandis, S.: Atmospheric Chemistry and Physics: From Air Pollution to Climate Change,
507 John Wiley, Hoboken, N. J., 1998.
508 Seinfeld, J. H., Bretherton, C. S., Carslaw, K. S., Coe, H., De- Mott, P. J., Dunlea, E. J., Feingold, G., Ghan,
509 S. J., Guenther, A.B., Kahn, R. A., Kracunas, I. P., Kreidenweis, S. M., Molina, M. J., Nenes, A.,
510 Penner, J. E., Prather, K. A., Ramanathan, V., Ramaswamy, V., Rasch, P. J., Ravishankara, A. R.,
511 Rosenfeld, D., Stephens, G., and Wood R.: Improving our fundamental understanding of the role of
512 aerosol-cloud interactions in the climate system, Proc. Nat. Acad. Sci. USA, 113, 5781–5790,
513 https://doi.org/10.1073/pnas.1514043113, 2016.
514 Sullivan, S.C., Lee, D., Oreopoulos, L., and Nenes, A.: The role of updraft velocity in temporal variability
515 of cloud hydrometeor number, Proc. Nat. Acad. Sci, 113, 21,
516 https://doi.org/10.1073/pnas.1514039113, 2016.
517 Wagner, N. L., Brock, C. A., Angevine, W. M., Beyersdorf, A., Campuzano-Jost, P., Day, D., de Gouw, J.
518 A., Diskin, G. S., Gordon, T. D., Graus, M. G., Holloway, J. S., Huey, G., Jimenez, J. L., Lack, D. A.,
519 Liao, J., Liu, X., Markovic, M. Z., Middlebrook, A. M., Mikoviny, T., Peischl, J., Perring, A. E.,
520 Richardson, M. S., Ryerson, T. B., Schwarz, J. P., Warneke, C., Welti, A., Wisthaler, A., Ziemba, L.
521 D., and Murphy, D. M.: In situ vertical profiles of aerosol extinction, mass, and composition over the
522 southeast United States during SENEX and SEAC4RS: observations of a modest aerosol enhancement
523 aloft, Atmos. Chem. Phys., 15, 7085-7102, https://doi.org/10.5194/acp-15-7085-2015, 2015.
524 Warneke, C., Trainer, M., de Gouw, J. A., Parrish, D. D., Fahey, D. W., Ravishankara, A. R., Middlebrook,
525 A. M., Brock, C. A., Roberts, J. M., Brown, S. S., Neuman, J. A., Lerner, B. M., Lack, D., Law, D.,
526 Hübler, G., Pollack, I., Sjostedt, S., Ryerson, T. B., Gilman, J. B., Liao, J., Holloway, J., Peischl, J.,

Nowak, J. B., Aikin, K. C., Min, K.-E., Washenfelder, R. A., Graus, M. G., Richardson, M., Markovic, M. Z., Wagner, N. L., Welti, A., Veres, P. R., Edwards, P., Schwarz, J. P., Gordon, T., Dube, W. P., McKeen, S. A., Brioude, J., Ahmadov, R., Bougiatioti, A., Lin, J. J., Nenes, A., Wolfe, G. M., Hanisco, T. F., Lee, B. H., Lopez-Hilfiker, F. D., Thornton, J. A., Keutsch, F. N., Kaiser, J., Mao, J., and Hatch, C. D.: Instrumentation and measurement strategy for the NOAA SENEX aircraft campaign as part of the Southeast Atmosphere Study 2013, Atmos. Meas. Tech., 9, 3063-3093, https://doi.org/10.5194/amt-9-3063-2016, 2016.

Wilson, J. C., Lafleur, B. G., Hilbert, H., Seebaugh, W. R., Fox, J., Gesler, D. W., Brock, C. A., Huebert, B. J., and Mullen, J.: Function and performance of a low turbulence inlet for sampling supermicron particles from aircraft platforms, Aerosol Sci. Tech., 38, 790–802, , https://doi.org/10.1080/027868290500841, 2004.

Weber RJ, Guo H, Russell AG, Nenes A.: High aerosol acidity despite declining atmospheric sulfate concentrations over the past 15 years, Nat. Geosci., 9, 282-285, https://doi.org/10.1038/ngeo2665, 2016.

Yu, S., Alapaty, K., Mathur, R., Pleim, J., Zhang, Y., Nolte, C., Eder, B., Foley, K., and Nagashima, T.: Attribution of the United States “warming hole”: Aerosol indirect effect and precipitable water vapor. Sci. Rep., 4, 6929, https:// doi.org/10.1038/srep06929, 2014.

Table 1: Research flights from the SENEX 2013 campaign used in this study. The symbol "☼" next to each flight number refers to daytime flight, and "☾" refers to a nighttime flight.

Flight	Date	Local Time (UTC-5)	Hygroscopicity Parameter κ	Organic mass fraction
4☼	10/6	09:55-16:30	0.23±0.02	0.62±0.11
5☼	11/6	11:30-17:57	0.20±0.00	0.68±0.05
6☼	12/6	09:48-15:31	0.21±0.01	0.68±0.07
9☾	19/6	17:30-23:29	0.24±0.01	0.66±0.06
10☼	22/6	10:01-17:09	0.21±0.02	0.68±0.08
11☼	23/6	10:08-17:22	0.25±0.03	0.58±0.07
12☼	25/6	10:18-17:25	0.39±0.02	0.35±0.18
14☼	29/6	10:26-17:39	0.22±0.03	0.62±0.07
15☾	2/7	20:08-02:51	0.28±0.05	0.55±0.09
16☾	3/7	19:56-02:55	0.22±0.05	0.67±0.09
17☼	5/7	09:52-16:24	0.23±0.05	0.59±0.14
18☼	6/7	09:19-16:18	0.31±0.02	0.52±0.08
19☼	8/7	10:11-16:44	0.23±0.04	0.62±0.08
Average			0.25±0.05	0.60±0.09

549 **Table 2:** Flight number, time interval, standard deviation of vertical wind velocity (σ_w) and characteristic
550 vertical velocity $w^*=0.79\sigma_w$ during flight segments where the aircraft flew at a constant altitude.

Flight (pass)	Time Interval (Local Time)	σ_w (m s^{-1})	w^* (m s^{-1})	Altitude a.s.l. (m)	Flight (pass)	Time Interval (Local Time)	σ_w (m s^{-1})	w^* (m s^{-1})	Altitude a.s.l. (m)
5 (1)	12:31-12:58	1.02	0.81	549± 58	9 (1)	18:44-18:58	0.25	0.20	797±2.01
5 (2)	13:16-13:29	0.82	0.65	982±11	9 (2)	19:20-19:29	0.25	0.2	740±1.23
5 (3)	13:34-13:50	1.01	0.80	502±13	9 (3)	19:33-19:48	0.22	0.17	740±1.23
5 (4)	13:53-14:08	1.03	0.81	614±27	9 (4)	19:51-20:25	0.22	0.17	776±1.22
5 (5)	14:20-15:00	0.91	0.72	603±40	9 (5)	20:34-20:39	0.23	0.18	597±1.19
5 (6)	15:35-15:41	0.87	0.69	533±18	9 (7)	20:56-21:10	0.20	0.16	773±1.11
5 (7)	16:17-16:30	0.77	0.61	638±23	9 (8)	21:31-21:45	0.19	0.15	725±1.18
5 (8)	16:31-16:39	0.55	0.44	559±18	9 (9)	22:24-22:31	0.26	0.20	745± 1.36
5 (9)	17:10-17:22	0.53	0.42	686±40	9 (10)	22:48-22:54	0.22	0.17	804± 1.37
14 (1)	12:34-12:49	0.94	0.75	558±2	15 (1)	21:09-21:52	0.24	0.19	505±6.64
14 (2)	13:57-14:17	0.97	0.77	658±3	15 (2)	22:19-22:31	0.30	0.24	633±1.21
14 (3)	14:22-14:46	0.95	0.75	737±3	15 (3)	22:42-22:54	0.25	0.20	600±1.17
14 (4)	14:58-15:33	0.55	0.43	746±23	15 (4)	23:26-23:37	0.33	0.26	908±1.56
14 (5)	15:55-16:08	0.57	0.45	714±3	15 (5)	00:02-00:19	0.30	0.23	1208±1.23
14 (6)	16:11-16:21	0.77	0.61	801±3	15 (6)	00:43-1:08	0.25	0.20	592±1.37
14 (7)	16:33-16:41	0.45	0.35	793± 2	15 (7)	1:10-1:24	0.28	0.22	676±1.02
					15 (8)	1:37-2:02	0.21	0.16	713±19.5
12 (1)	11:50-12:34	0.96	0.75	484±3	19 (1)	11:20-11:41	0.62	0.49	1014±2.27
12 (2)	12:48-13:18	1.09	0.86	503±3	19 (2)	12:09-12:23	1.20	0.95	652±3.34
12 (3)	13:34-13:50	1.12	0.88	894±3	19 (3)	12:51-13:10	0.87	0.69	537±2.51
12 (4)	14:06-14:40	1.04	0.82	479±4	19 (4)	13:22-13:49	1.29	1.02	518±22.6
12 (5)	15:21-15:32	1.10	0.87	521±3	19 (5)	14:44-14:57	1.36	1.07	528±3.26
12 (6)	15:43-16:02	0.99	0.78	475±3	19 (6)	15:04-16:06	0.90	0.71	524±2.8

551

552

Table 3: Derived cloud parameters (maximum supersaturation, droplet number) and relative contribution of chemical composition and total aerosol number for different vertical velocities. Numbers in parentheses indicate standard deviation values. The symbol "☼" next to each flight number refers to daytime flight, and "☾" refers to a nighttime flight.

Flight	N_a	*Std Dev* N_a	σ_w=0.1 m s^{-1}				σ_w=0.3 m s^{-1}				σ_w=0.6 m s^{-1}				σ_w=1.0 m s^{-1}			
			S_{max}	N_d	Contrib κ	Contrib N_a	S_{max}	N_d	Contrib κ	Contrib N_a	S_{max}	N_d	Contrib κ	Contrib N_a	S_{max}	N_d	Contrib κ	Contrib N_a
4☼	6118	4520	0.11 (0.06)	122 (41)	0.08	0.92	0.16 (0.09)	315 (114)	0.20	0.80	0.21 (0.12)	520 (212)	0.23	0.77	0.26 (0.17)	737 (321)	0.2	0.8
5☼	4324	2598	0.08 (0.04)	139 (31)	0.09	0.91	0.1 (0.06)	388 (104)	0.15	0.85	0.14 (0.08)	712 (216)	0.17	083	0.17 (0.1)	1063 (360)	0.21	0.79
6☼	4958	3054	0.07 (0.07)	151 (24)	0.03	0.97	0.08 (0.04)	422 (70)	0.11	0.89	0.1 (0.06)	773 (171)	0.08	0.92	0.13 (0.07)	1162 (302)	0.07	0.93
9☾	4271	3095	0.07 (0.02)	152 (18)	0.05	0.95	0.12 (0.04)	367 (68)	0.17	0.83	0.16 (0.05)	533 (115)	0.17	0.83	0.19 (0.06)	680 (126)	0.12	0.88
10☼	6286	7201	0.07 (0.03)	158 (24)	0.02	0.98	0.1 (0.05)	422 (86)	0.02	0.98	0.14 (0.07)	748 (180)	0.04	0.96	0.18 (0.08)	1063 (295)	0.09	0.91
11☼	5969	7271	0.04 (0.01)	137 (19)	0.01	0.99	0.06 (0.01)	381 (61)	0.04	0.96	0.08 (0.02)	695 (134)	0.03	0.97	0.10 (0.02)	1025 (226)	0.03	0.97
12☼	3154	5150	0.06 (0.03)	110 (45)	0.03	0.97	0.1 (0.04)	274 (117)	0.05	0.95	0.14 (0.04)	404 (179)	0.08	0.92	0.17 (0.05)	486 (207)	0.07	0.93
14☼	5564	5891	0.07 (0.02)	118 (41)	0.05	0.95	0.10 (0.03)	328 (125)	0.17	0.83	0.13 (0.04)	590 (240)	0.25	0.75	0.16 (0.05)	842 (361)	0.27	0.73
15☾	2328	1428	0.05 (0.01)	135 (22)	0.03	0.97	0.09 (0.02)	339 (67)	0.12	0.88	0.12 (0.02)	557 (137)	0.21	0.79	0.16 (0.03)	717 (203)	0.3	0.7
16☾	3440	4507	0.08 (0.06)	158 (37)	0.03	0.97	0.12 (0.1)	403 (120)	0.06	0.94	0.17 (0.13)	670 (235)	0.07	0.93	0.23 (0.16)	917 (374)	0.1	0.9
17☼	3813	4645	0.05 (0.02)	129 (41)	0.06	0.94	0.07 (0.03)	342 (130)	0.1	0.9	0.1 (0.04)	593 (248)	0.06	0.94	0.13 (0.05)	841 (371)	0.06	0.94
18☼	1925	983	0.08 (0.04)	90 (58)	0.12	0.88	0.12 (0.05)	233 (157)	0.35	0.65	0.15 (0.06)	379 (262)	0.37	0.63	0.19 (0.07)	499 (346)	0.27	0.73
19☼	4323	7261	0.06 (0.02)	121 (33)	0.02	0.98	0.08 (0.02)	314 (96)	0.06	0.94	0.12 (0.03)	526 (177)	0.11	0.89	0.15 (0.03)	670 (249)	0.13	0.87

559 **Table 4:** Derived S_{max}, N_d, σ_w for all research flights along with the estimated contribution of each
560 parameter to the variability of the droplet number. The symbol "☼" next to each flight number refers to
561 daytime flight, and "☾" refers to a nighttime flight.

Flight	σ_w **(m s^{-1})**	$\frac{\Delta\sigma_w}{\sigma_w}$	S_{max} **(%)**	N_d **(cm^{-3})**	$\frac{\Delta N_d}{N_d}$	**Contrib. κ**	**Contrib. N_a**	**Contrib. σ_w**
4☼	1.03±0.25	0.243	0.29±0.19	707±343	0.485	4%	79%	17%
5☼	0.97±0.1	0.103	0.17±0.10	1040±350	0.337	7%	69%	24%
6☼	0.94±0.18	0.191	0.13±0.07	1108±283	0.255	3%	54%	43%
9☾	0.23±0.02	0.043	0.10±0.03	309±51	0.165	7%	76%	17%
10☼	1.22±0.11	0.090	0.12±0.03	1177±271	0.230	1%	90%	9%
11☼	1.08±0.04	0.037	0.11±0.03	1082±242	0.224	1%	83%	16%
12☼	1.05±0.07	0.067	0.18±0.05	495±210	0.424	2%	96%	2%
14☼	0.85±0.2	0.024	0.15±0.04	761±321	0.422	9%	72%	19%
15☾	0.28±0.04	0.143	0.08±0.02	321±63	0.196	7%	51%	42%
16☾	0.20±0.04	0.200	0.10±0.08	289±79	0.273	2%	65%	33%
17☼	0.71±0.26	0.366	0.15±0.11	742±280	0.377	1%	71%	28%
18☼	0.90±0.06	0.067	0.31±0.18	538±325	0.604	7%	83%	10%
19☼	0.99±0.31	0.313	0.15±0.03	699±248	0.355	4%	88%	8%
Average					0.334	4%	75.2%	20.6%

562

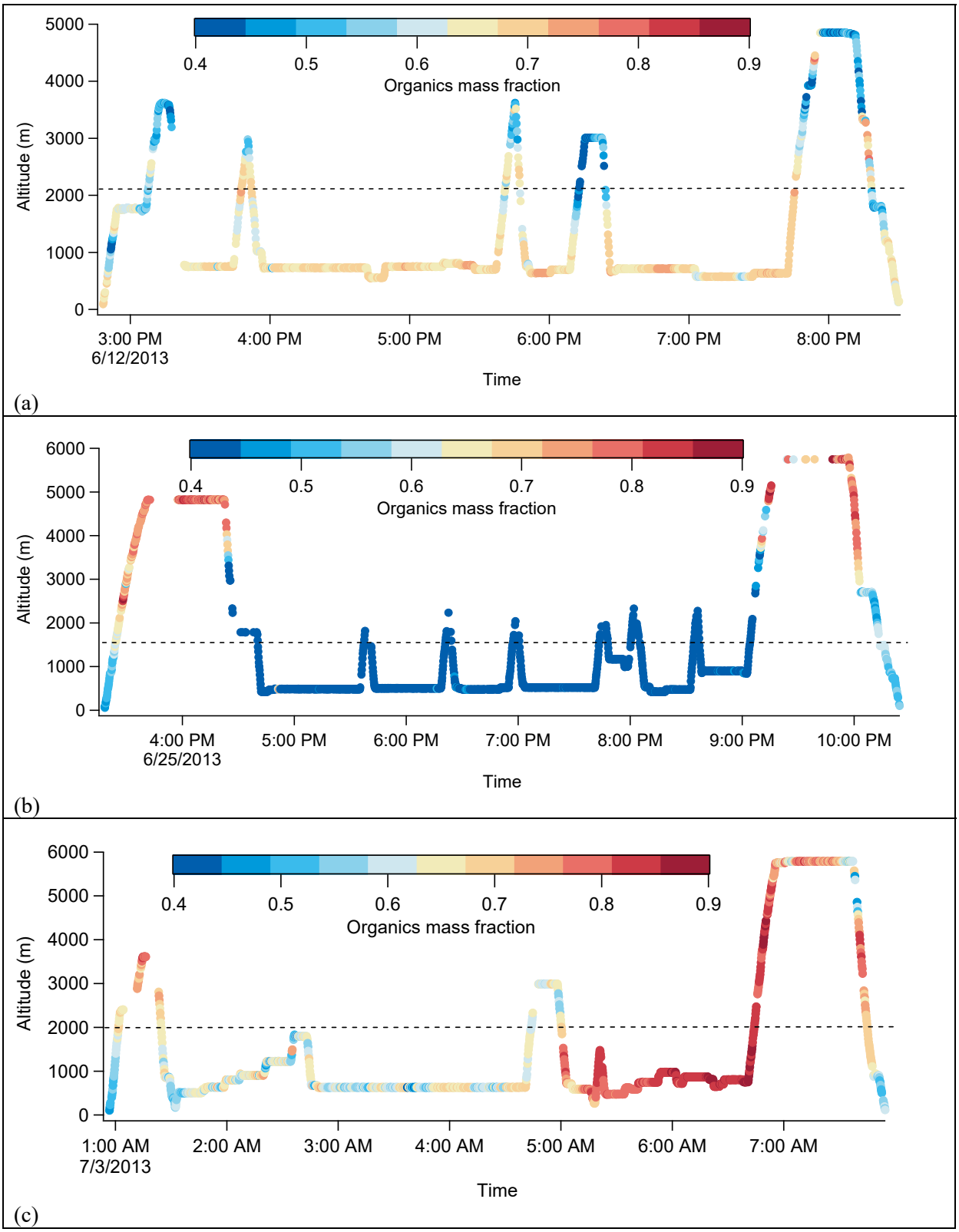

563 **Figure 1:** Altitude as a function of time (UTC) colored by organic mass fraction. Spatial and vertical
564 distribution of the organics mass fraction (a) for Flight 6, (b) for Flight 12 and (c) for Flight 16, denoting

565 the difference in chemical composition, which in turn, may influence cloud droplet number concentration.
566 The dashed line represents the boundary layer height.

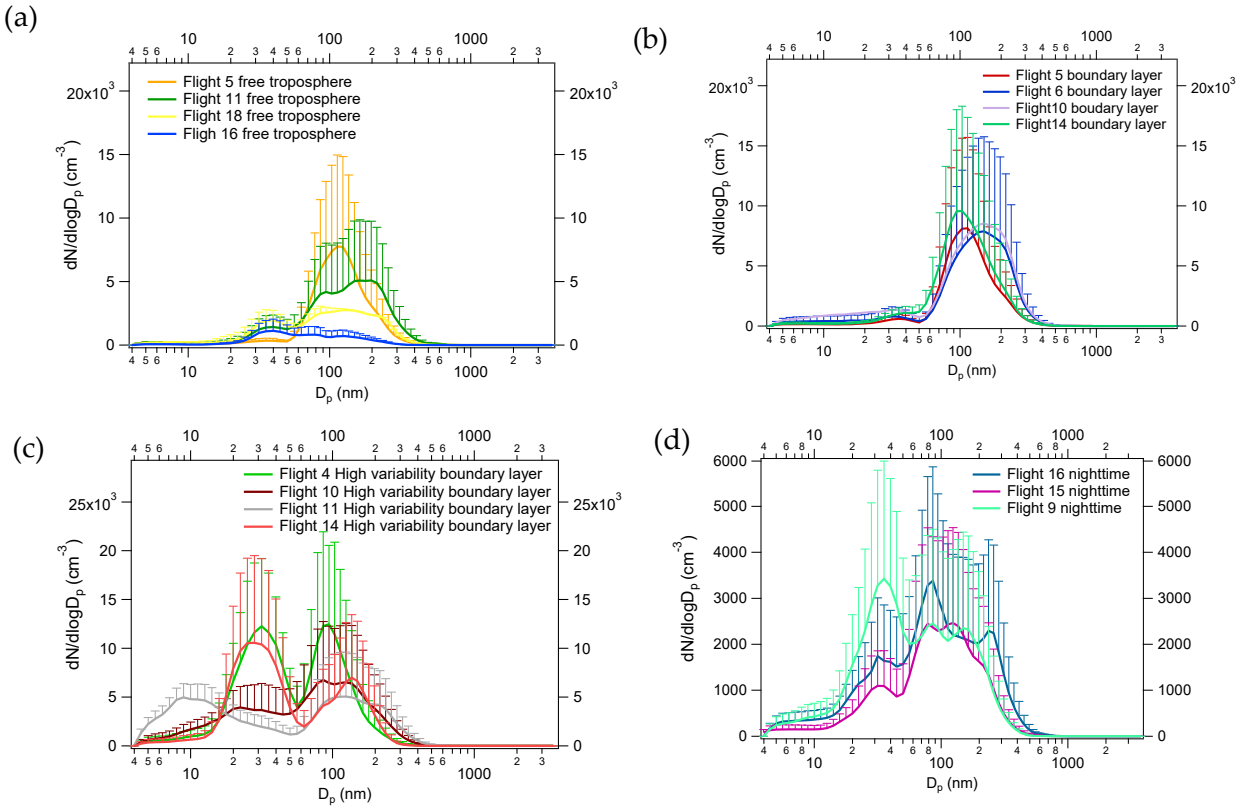

567

568 **Figure 2:** Average particle number size distributions for: (a) free tropospheric conditions, (b) within the
569 boundary layer, (c) during segments with high variability in total aerosol number, and (d) during nighttime
570 passes. Error bars represent the 75th percentile of the distributions within each segment.

571

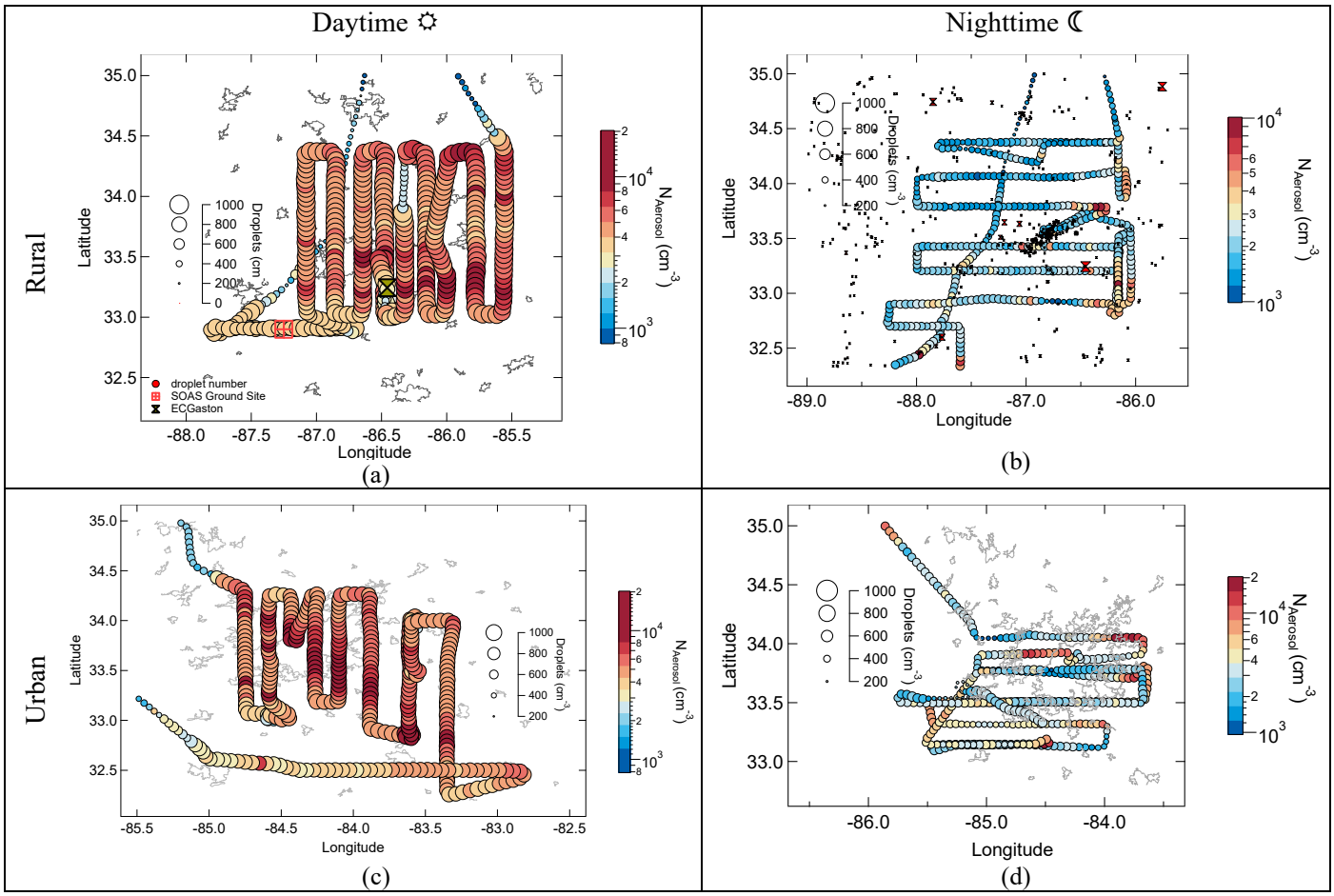

572

573 **Figure 3:** Map of aircraft flight track showing calculated cloud droplet number (indicated by marker size
574 (cm^{-3})) and total aerosol number (indicated by marker color) for the observed characteristic vertical velocity
575 (w^*). (a) for the rural sector during daytime (Flight 5) and (b) nighttime (Flight 15). (c) for urban Atlanta
576 during daytime (Flight 6) and (d) nighttime (Flight 9). Note that the data are plotted at less than 1 Hz in
577 order to better show the size and color of the markers.

578

579

580

581

582

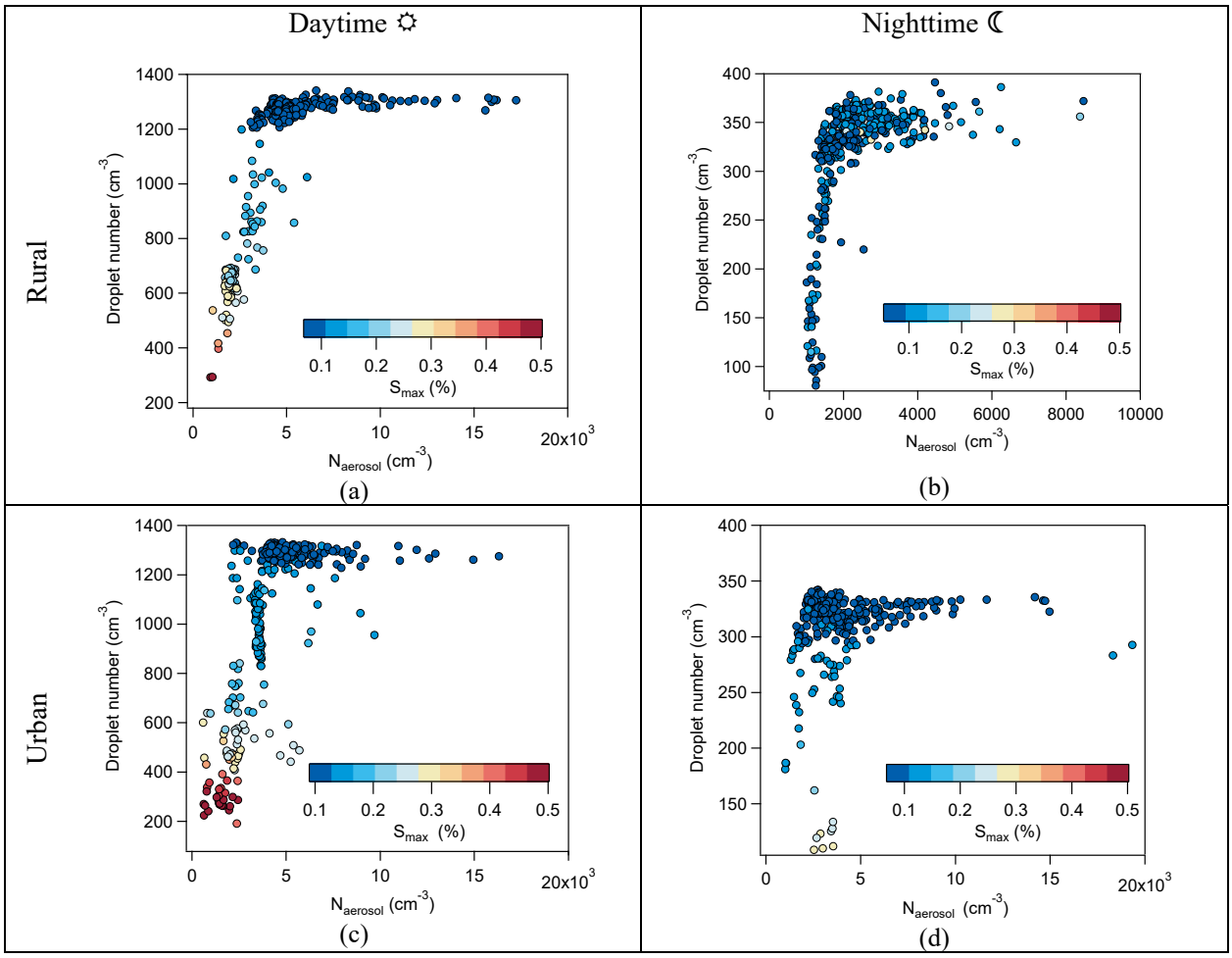

Figure 4: Cloud droplet number vs. total aerosol number for the derived characteristic vertical velocity (w^*) of each flight (Table 4). (a) for the rural sector during daytime (Flight 5) and (b) nighttime (Flight 15). (c) for urban Altanta during daytime (Flight 6) and (d) nighttime (Flight 9). Data are colored by maximum supersaturation.

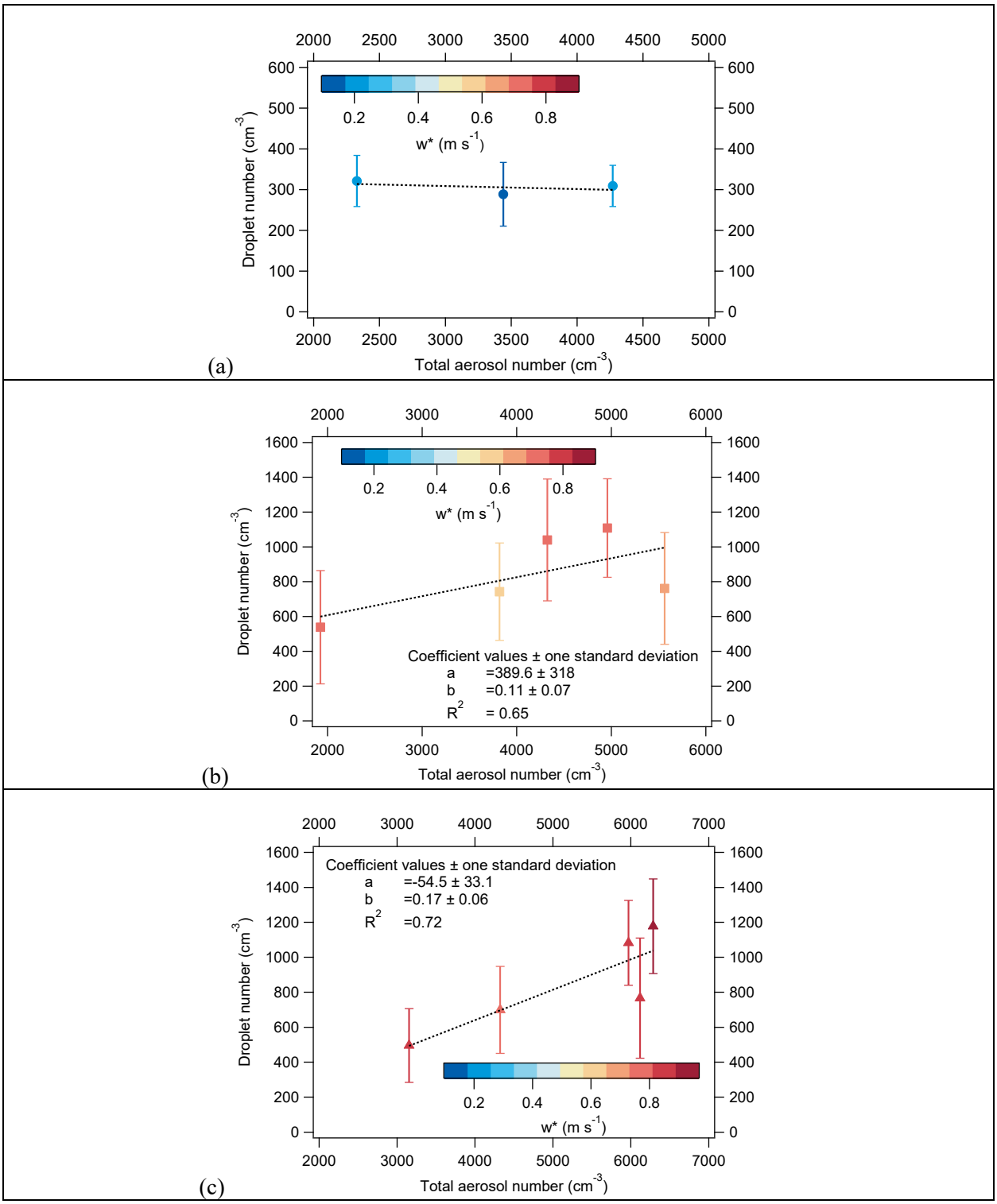

Figure 5: Average cloud droplet number vs. total aerosol number, colored by characteristic velocity w* for each flight. Error bars represent the standard deviation of cloud droplet number during each flight.

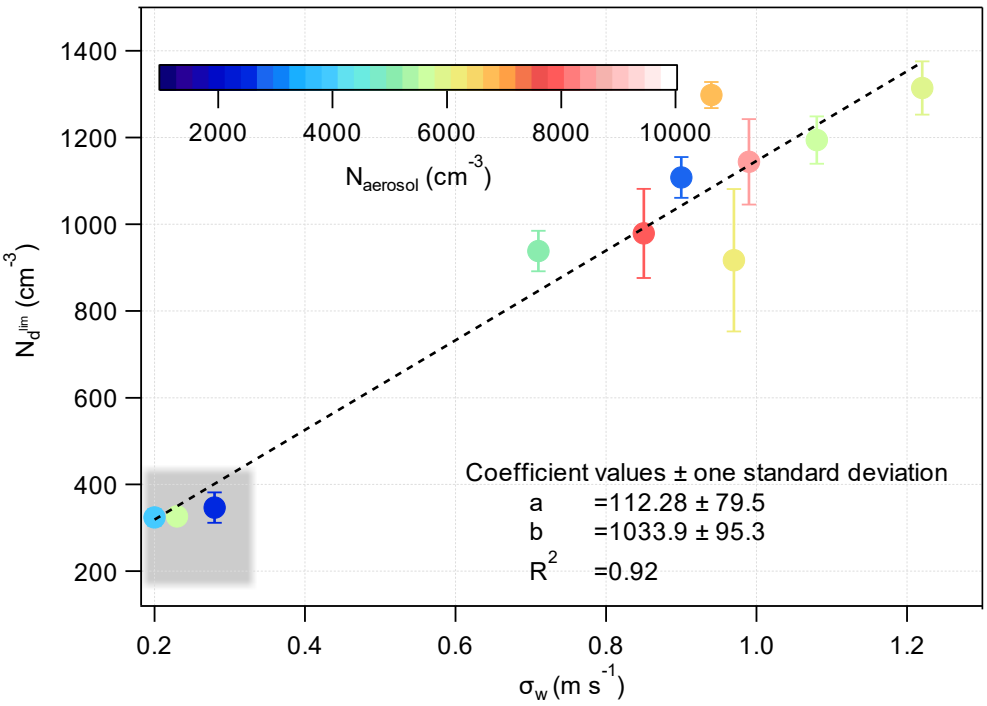

Figure 6: Limiting droplet number vs. standard deviation of vertical velocity during flights where a velocity-limited regime is reached (all except Flights 4, 12). The shaded area represents the segments of the flights conducted during nighttime while color scale denotes total aerosol number levels.